QUANTUM MECHANICS

10.1126/sciadv.1501165

Engineering two-photon high-dimensional states through quantum interference

Yingwen Zhang,[1] Filippus S. Roux,[1,2] Thomas Konrad,[3,4] Megan Agnew,[5] Jonathan Leach,[5] Andrew Forbes[2]*

Many protocols in quantum science, for example, linear optical quantum computing, require access to large-scale entangled quantum states. Such systems can be realized through many-particle qubits, but this approach often suffers from scalability problems. An alternative strategy is to consider a lesser number of particles that exist in high-dimensional states. The spatial modes of light are one such candidate that provides access to high-dimensional quantum states, and thus they increase the storage and processing potential of quantum information systems. We demonstrate the controlled engineering of two-photon high-dimensional states entangled in their orbital angular momentum through Hong-Ou-Mandel interference. We prepare a large range of high-dimensional entangled states and implement precise quantum state filtering. We characterize the full quantum state before and after the filter, and are thus able to determine that only the antisymmetric component of the initial state remains. This work paves the way for high-dimensional processing and communication of multiphoton quantum states, for example, in teleportation beyond qubits.

INTRODUCTION

It is now well understood that an increase in the dimensionality of quantum systems is beneficial; for example, it gives higher security in communication systems and increases transmission rates (*1*–*3*). There are many routes to realizing high-dimensional quantum states, using various degrees of freedom, such as time-energy (*4*), paths (*5*), the use of spatial modes (*6*–*9*), and combinations thereof (*10*, *11*). In particular, the entanglement of photons that carry orbital angular momentum (OAM) has generated much interest in recent years (*12*, *13*). Although OAM has been mooted as a means of realizing high-dimensional state spaces, very little work has actually demonstrated this [but see, for instance, Mafu *et al.* (*14*)].

Recently, the use of OAM modes has been proposed to implement teleportation of high-dimensional quantum states (*15*, *16*), so-called qudits, and the teleportation of spin-orbit hyper-entangled photons has been demonstrated in Wang *et al.* (*17*) and Graham *et al.* (*18*). High-capacity teleportation channels are an essential ingredient to enable long-distance quantum communication by means of quantum repeaters (*19*). However, teleportation based on Bell filters for OAM entanglement using linear optics requires a filter for antisymmetric states (*16*).

Hong-Ou-Mandel (HOM) interference (*20*) is a fundamental component in many quantum information protocols and one of the defining features of quantum physics. When each of the two input ports of a 50:50 beamsplitter receives one photon, only the antisymmetric state component and not the symmetric one produces coincidence counts in the output ports. This has been demonstrated for incident pairs of photons prepared in symmetric and antisymmetric states involving two spatial modes (*21*–*23*). HOM interference was investigated for various scenarios, for example, in polarization (*24*), in path length (*25*), in the radial dependence of the light field in a transversal plane (*26*), in spectral filtering (*27*), for different single-photon sources (*28*), and with spatial modes (*23*, *29*–*31*). Generalizations to higher photon number and multiport as well as realizations with other bosonic systems (*32*) have been discussed in the literature. The HOM effect is applied not only to characterize single-photon sources (*33*) but also in the construction of quantum logic gates (*34*), quantum cloning (*35*–*38*), and phase shaping of single photons (*39*). In the context of OAM, no study to date has demonstrated the preparation of a high-dimensional quantum state by HOM interference.

Here, we extend the concept of HOM interference to photons entangled in more than two spatial modes, implementing a HOM measurement for OAM states. For the first time, we experimentally verify by state tomography that conditioning on coincident counts leads to a projection onto an antisymmetric state carrying high-dimensional entanglement. This filter (when conditioned on coincidences at the detector) for antisymmetric states can also act as a sorter for odd and even OAM states, and we show that coincidence counts will be produced by odd OAM states whereas double counts are produced by even states. This is the first reported observation of HOM interference for high-dimensional OAM entangled states and could enable quantum teleportation of qudits, as well as high-dimensional implementations of dense coding and other quantum technologies that rely on measurements of nonlocal observables.

RESULTS

We begin by generating high-dimensional entangled photon pairs (see Materials and Methods). We use a laser to pump a nonlinear crystal to generate spontaneous parametric down-conversion (SPDC). At the exit facet of the crystal, SPDC produces the state (*6*)

$$|\Psi\rangle = \sum_{\ell=1}^{\infty} a_\ell |\Psi_\ell^+\rangle \tag{1}$$

where $|\Psi_\ell^+\rangle$ are symmetric OAM Bell states $(|\ell\rangle_A|-\ell\rangle_B + |-\ell\rangle_A|\ell\rangle_B)/\sqrt{2}$, and α_ℓ is a complex coefficient in the expansion. Here $|\ell\rangle$ represents a photon with an OAM of $\ell\hbar$. Here, we do not consider the contribution from $\ell = 0$. The subscripts A and B label the photon path. Note that the photons are entangled in momentum, owing to the phase matching

[1]Council for Scientific and Industrial Research (CSIR) National Laser Centre, PO Box 395, Pretoria 0001, South Africa. [2]School of Physics, University of Witwatersrand, Johannesburg 2000, South Africa. [3]School of Chemistry and Physics, University of KwaZulu-Natal, Private Bag X54001, Durban 4000, South Africa. [4]National Institute for Theoretical Physics, University of KwaZulu-Natal, Private Bag X54001, Durban 4000, South Africa. [5]Institute of Photonics and Quantum Science (IPaQS), Scottish Universities Physics Alliance (SUPA), Heriot-Watt University, Edinburgh EH14 4AS, UK.
*Corresponding author. E-mail: andrew.forbes@wits.ac.za

condition of the crystal. In the OAM basis, the photon states are anticorrelated: because the pump has zero OAM, the sum of the OAM of photons A and B must also add to zero, hence the superposition state of Eq. 1.

For the purpose of this work, it is necessary to generate high-dimensional entangled states that have both symmetric and antisymmetric contributions; this is achieved with Dove prisms. A pair of Dove prisms oriented at an angle ϕ with respect to each other introduces a phase factor that is proportional to the OAM index of the state $|\ell\rangle \rightarrow |\ell\rangle \exp(i2\ell\phi)$. The effect on an individual subspace is

$$|\Psi_\ell^+\rangle \rightarrow |\Psi_\ell\rangle = \frac{1}{\sqrt{2}}\left(|\ell\rangle_A|-\ell\rangle_B e^{i2\ell\phi} + |-\ell\rangle_A|\ell\rangle_B e^{i2\ell\phi}\right)$$
$$= \frac{1}{\sqrt{2}}\left(|\Psi_\ell^+\rangle\cos(2\ell\phi) + i|\Psi_\ell^-\rangle\sin(2\ell\phi)\right) \quad (2)$$

It follows that with an appropriate choice of ϕ, the high-dimensional entangled state in Eq. 1 can be converted into a state with symmetric and antisymmetric contributions (*40*). For example, after passing through two Dove prisms with $\phi = \pi/4$, every subspace in Eq. 1 with an even OAM value will remain symmetric $|\Psi^+_{\ell\ \mathrm{even}}\rangle \rightarrow |\Psi^+_{\ell\ \mathrm{even}}\rangle$, and every subspace with an odd OAM value will become antisymmetric $|\Psi^+_{\ell\ \mathrm{odd}}\rangle \rightarrow |\Psi^-_{\ell\ \mathrm{odd}}\rangle$. The Dove prisms will introduce additional phases between the subspaces, but in this experiment, these phases do not play a significant role.

Additionally, the $|\Phi_\ell^\pm\rangle$ states and any superposition thereof can be generated by inserting a third Dove prism into one of the photon paths

$$|\Psi_\ell^+\rangle \rightarrow |\Phi_\ell\rangle = \frac{1}{\sqrt{2}}\left(|\ell\rangle_A|\ell\rangle_B e^{i2\ell\phi} + |-\ell\rangle_A|-\ell\rangle_B e^{i2\ell\phi}\right)$$
$$= \frac{1}{\sqrt{2}}\left(|\Phi_\ell^+\rangle\cos(2\ell\phi) + i|\Phi_\ell^-\rangle\sin(2\ell\phi)\right) \quad (3)$$

The filter for high-dimensional OAM entangled states comprises a 50:50 beamsplitter in combination with two mirrors (see the beige region in Fig. 1). The mirrors are necessary because of the reflection at the beamsplitter that causes a change of sign of the OAM value. They serve to invert the OAM value both before and after the beamsplitter and ensure that the combined system acts as a traditional HOM filter; that is, it is the antisymmetric input state that is unchanged on propagation. In this sense, we have a filter so long as we condition on coincidences at the detection point.

We identify three cases describing the action of the filter: the first is when the input state is $|\Psi_\ell\rangle$, the second is when the state is $|\Phi_\ell\rangle$, and the final case is the general case of a high-dimensional entangled state composed of a superposition of OAM Bell states. When the input state is $|\Psi_\ell\rangle$ (Eq. 2), the output from the mirrors and beamsplitter are given by (see Supplementary Materials)

$$|\Psi_{\mathrm{out}}\rangle = \frac{1}{\sqrt{2}}[(|\ell\rangle_{A'}|-\ell\rangle_{B'} - |-\ell\rangle_{A'}|-\ell\rangle_{B'})i\sin(2\ell\phi)$$
$$-(|\ell\rangle_{A'}|-\ell\rangle_{A'}|-\ell\rangle_{B'}|-\ell\rangle_{B'})\cos(2\ell\phi)] \quad (4)$$

This output state has two components. The first part is simply the antisymmetric state, with one photon in each path A′ and B′, resulting in the detection of coincidence counts. The second part corresponds to a superposition of two photons in path A′ or two photons in path B′, resulting in no coincidence counts. As the antisymmetric component is weighted by the factor $i\sin(2\ell\phi)$, we will observe maximal coincidence counts for $\phi = \pi(1+2n)/(4\ell)$ for any integer n. Conversely, we will observe no coincidence counts for $\phi = n\pi/(2\ell)$.

When the input state is $|\Phi_\ell\rangle$ (Eq. 3), the output from the mirrors and beamsplitter will be given by (see Supplementary Materials)

$$|\Psi_{\mathrm{out}}\rangle = \frac{1}{\sqrt{2}}[(|\ell\rangle_{A'}|\ell\rangle_{A'} - |\ell\rangle_{B'}|\ell\rangle_{B'})\exp(i2\ell\phi)$$
$$+(|-\ell\rangle_{A'}|-\ell\rangle_{A'} - |-\ell\rangle_{B'}|-\ell\rangle_{B'})\exp(-i2\ell\phi)] \quad (5)$$

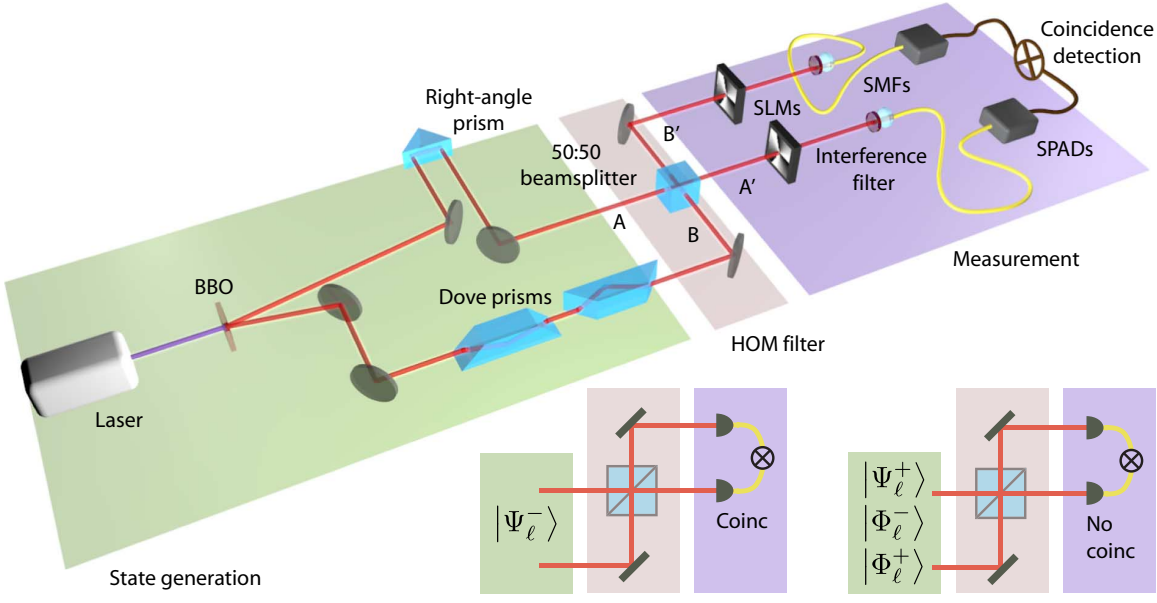

Fig. 1. Diagram of the experimental setup used to demonstrate high-dimensional HOM interference. The HOM filter, indicated by the beige section, consists of two mirrors and a 50:50 beamsplitter. Any antisymmetric state $|\Psi_\ell^-\rangle$ will result in one photon in each of the modes A′ and B′ and the detection of coincidences; any symmetric state $|\Psi_\ell^+\rangle$, $|\Phi_\ell^+\rangle$, or $|\Phi_\ell^-\rangle$ will result in a superposition of two photons in either A′ or B′ and the absence of a coincidence signal. SLM, spatial light modulator; SPAD, single-photon avalanche detector; SMF, single-mode optical fiber.

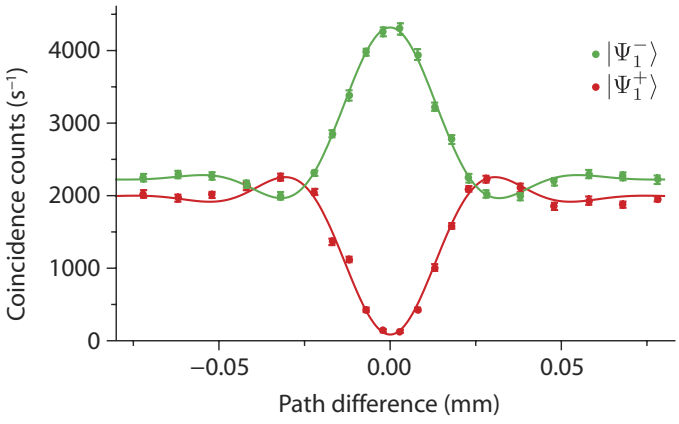

Fig. 2. Photon coincidence counts measured as a function of the path length difference. The red points denote input states $|\Psi_\ell^+\rangle$, and the green points denote input states $|\Psi_\ell^-\rangle$. We observe a HOM interference dip/peak when the path length difference is equal to zero. The data points shown are the average of 20 readings. A Gaussian function multiplied by a sinc function was fitted to the data and is shown as solid curves.

Both components of this output state correspond to a superposition of two photons in path A′ or two photons in path B′, resulting in no coincidence counts regardless of the value of ϕ. Thus, we see that the combination of the mirrors and the beamsplitter acts as a filter that only allows the antisymmetric OAM Bell state $|\Psi_\ell^-\rangle$ to pass when conditioned on a coincidence detection of photons in paths A′ and B′.

The final case that we consider is the general description of a high-dimensional entangled state; any such state can be decomposed into a superposition of OAM Bell states

$$\sum_\ell [a_\ell|\Phi_\ell^+\rangle + b_\ell|\Phi_\ell^-\rangle + c_\ell|\Psi_\ell^+\rangle + d_\ell|\Psi_\ell^-\rangle] \quad (6)$$

This state is composed of two parts: a symmetric part $|s^+\rangle$, which contains $|\Phi_\ell^+\rangle$, $|\Phi_\ell^-\rangle$, and $|\Psi_\ell^+\rangle$, and an antisymmetric part $|s^-\rangle$, which contains $|\Psi_\ell^-\rangle$. If this state is incident on the filter, only the antisymmetric component $|\Psi_\ell^-\rangle$ of the state remains unchanged and can be detected in coincidence. See eq. S5 for further details.

To test the filter, we characterize its performance for entangled OAM modes. Figure 2 shows HOM interference for the symmetric input state $|\Psi_1^+\rangle$ and antisymmetric input state $|\Psi_1^-\rangle$. We change the path difference between paths A and B and record a dip in the coincidence rate for the $|\Psi_1^+\rangle$ input state and a peak in the coincidence rate for the $|\Psi_1^-\rangle$. The symmetric state $|\Psi_1^+\rangle$ is produced when the angle between the Dove prisms is set to $\phi = 0$; the antisymmetric state $|\Psi_1^-\rangle$ is produced when the angle between the Dove prisms is set to $\phi = \pi/4$. For the $|\Psi_1^-\rangle$ input state, we observe an increase in the coincidence rate by a factor of 2 when the path difference is zero, corresponding to quantum interference characteristic of the antisymmetric state. A Gaussian function multiplied by a sinc function is fitted to the experimental data. The fitting function depends on the bandwidth of the interference filters and the difference in optical path (*41*).

Figure 3A shows the coincidences detected as a function of angle ϕ between the Dove prisms for the input states $|\Psi_1\rangle$ and $|\Phi_1\rangle$; these are specific cases of Eq. 6. As ϕ varies, the superposition of input states changes, resulting in higher or lower coincidences based on the value of d_1. The green points correspond to a superposition of $|\Psi_1^+\rangle$ and

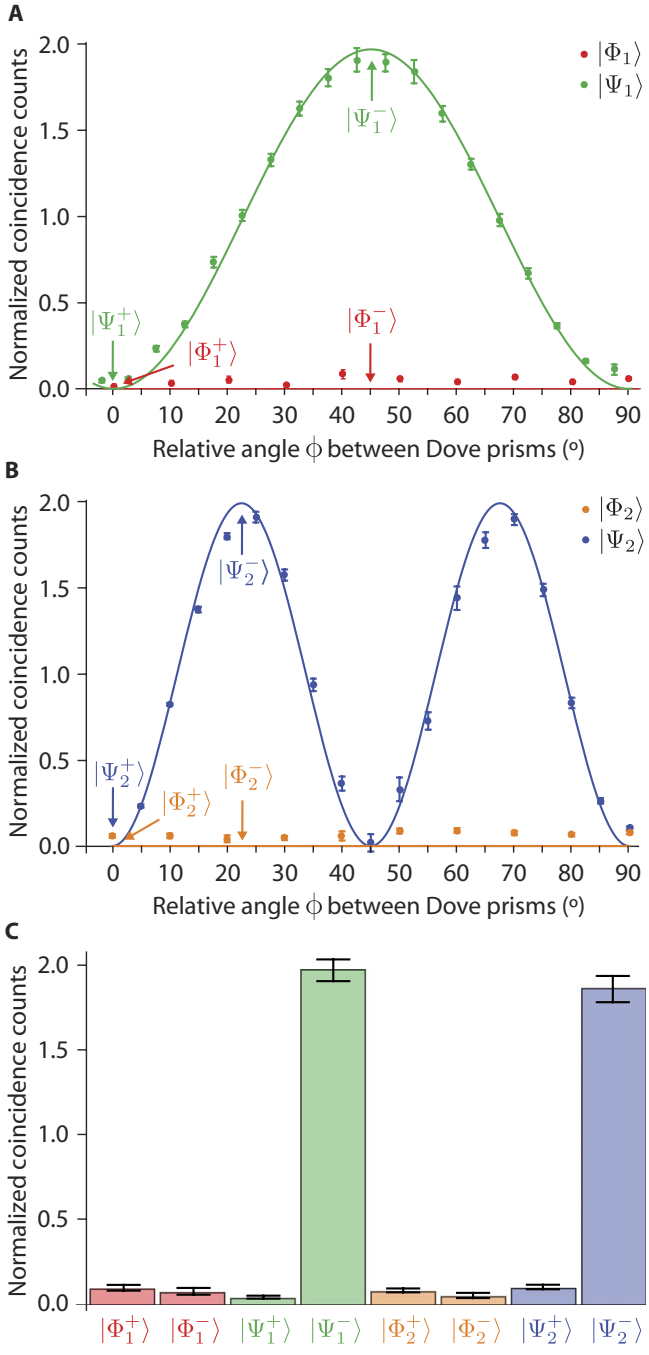

Fig. 3. Coincidence counts as a function of input state. (**A**) Graph showing the variation of coincidence counts for the input states $|\Psi_1\rangle$, indicated by the green points, and $|\Phi_1\rangle$, indicated by the red points. The theoretical variation in coincidence counts of any $|\Psi_1\rangle$ input state is equal to 2 $\sin^2(2\phi)$. For any $|\Phi_1\rangle$ input state, the coincidence counts should remain zero as a function of ≻. The normalized count rate is determined by dividing the coincidence rate in the dip/peak by that outside of the dip/peak. The error bars represent 1 SD from averaging 20 readings. (**B**) Graph showing the variation of coincidence counts for the input states $|\Psi_2\rangle$, indicated by the blue points, and $|\Phi_2\rangle$, indicated by the orange points. The theoretical variation in coincidence counts of any $|\Psi_2\rangle$ input state is equal to 2 $\sin^2(4\phi)$. (**C**) Normalized coincidence counts for the OAM $\ell = 1$ and 2 Bell states. Only the $|\Psi_1^-\rangle$ and $|\Psi_2^-\rangle$ input states result in coincidences being recorded.

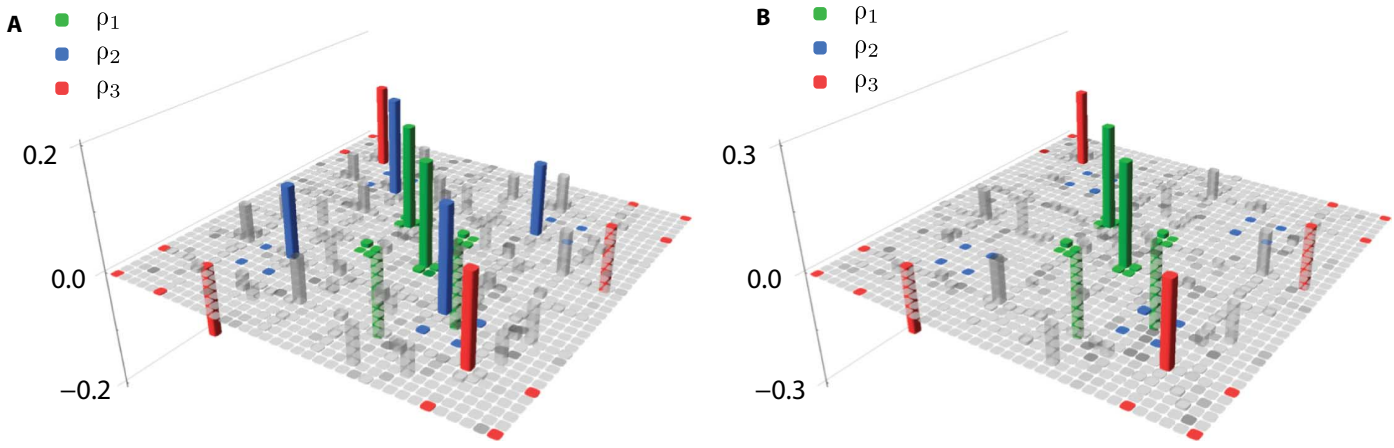

Fig. 4. The high-dimensional density matrices corresponding to the state before and after the filter. Only the real parts of the density matrices are shown. (**A**) The state before the filter, which in principle is given by $d_1|\Psi_1^-\rangle + c_2|\Psi_2^+\rangle + d_3|\Psi_3^-\rangle$; there is a strong contribution from the $\ell = 1$, 2, and 3 subspaces in this six-dimensional state (36 × 36 matrix). (**B**) The state after the filter, which in principle is given by $d_1'|\Psi_1^-\rangle + d_3'|\Psi_3^-\rangle$; the contribution from the $\ell = 2$ subspace is 3.8 ± 0.2% of its original value.

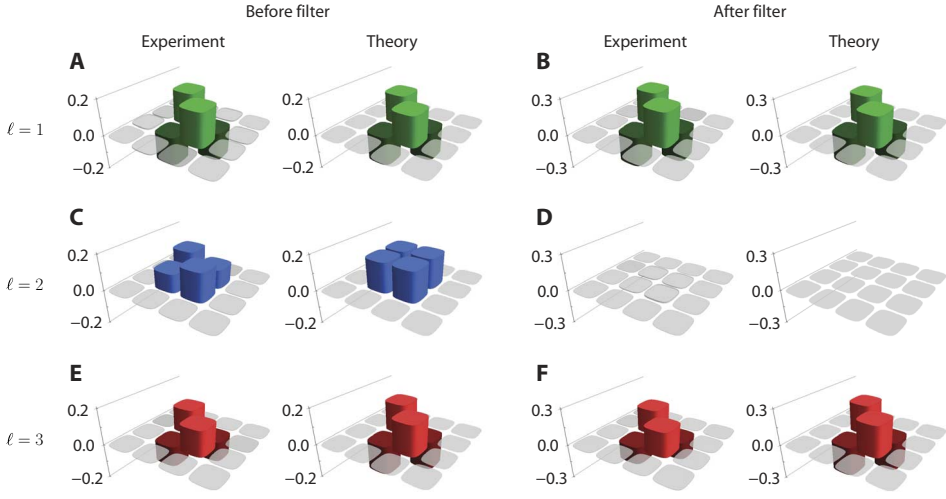

Fig. 5. A comparison of the density matrices of the individual two-dimensional subspaces extracted from Fig. 4. Only real parts are shown in this 4 × 4 matrix of the two-dimensional subspace. (**A** to **F**) The first two columns (A, C, and E) show the subspaces before the filter; the final two columns (B, D, and F) show the subspaces after the filter. Experimental results are shown in the left column of each pair, and theoretical predictions are shown in the right column of each pair. The $\ell = 1$ subspace is shown in green, $\ell = 2$ in blue, and $\ell = 3$ in red. Darker bars indicate negative values, whereas gray bars indicate absolute values less than 0.05.

Table 1. The trace of each subspace ρ_ℓ before and after the filter. This provides the probability of projecting onto a particular subspace spanned by the states with OAM values $\pm\ell$.

Subspace	Tr[ρ_ℓ] before the filter	Tr[ρ_ℓ] after the filter
ρ_1	0.370 ± 0.002	0.556 ± 0.001
ρ_2	0.319 ± 0.002	0.018 ± 0.001
ρ_3	0.278 ± 0.002	0.409 ± 0.001

$|\Psi_1^-\rangle$, whereas the red points correspond to a superposition of $|\Phi_1^+\rangle$ and $|\Phi_1^-\rangle$. Because the red data have only symmetric states in the superposition, no value of ϕ produces coincidences; conversely, the green data have a nonzero antisymmetric component, and the coincidence rate varies as $2\sin^2(2\ell\phi)$. These data show that the filter can project out the antisymmetric component from a two-dimensional OAM space. In addition to this result, Fig. 3B shows the coincidences detected as a function of angle ϕ between the Dove prisms for the input states $|\Psi_2\rangle$ and $|\Phi_2\rangle$. At $\phi + \pi/4$, the filter can act as an odd and even OAM sorter. At $\phi + \pi/4$, all the odd OAM states will be in the $|\Psi_\ell^-\rangle$

state, thereby giving only coincidence counts, whereas all the even states will be in the $|\Psi_\ell^+\rangle$ and will give only double counts.

Finally, we consider the high-dimensional input state of Eq. 6 with OAM values ℓ = 1, 2, and 3. By setting the angle $\phi = \pi/4$ between the two Dove prisms, we produce a high-dimensional state with both symmetric and antisymmetric components. We are able to select after the filter which subspaces to analyze, and we therefore consider only the input state $|\Psi_{in}\rangle = d_1|\Psi_1^-\rangle + c_2|\Psi_2^+\rangle + d_3|\Psi_3^-\rangle$. Upon propagation through the filter, the antisymmetric subspaces are the only ones that remain unchanged, and the renormalized state detected in coincidence is $d'_1|\Psi_1^-\rangle + d'_3|\Psi_3^-\rangle$.

We perform full state tomography (*42*) before and after the filter and reconstruct the high-dimensional density matrices ρ associated with the states; these are shown in Fig. 4. The ℓ = 1 subspace is highlighted in green, ℓ = 2 in blue, and ℓ = 3 in red. After the filter, the blue subspace has effectively been filtered out and has only near-zero values, whereas the red and green subspaces remain unchanged.

Figure 5 shows the density matrices of the two-dimensional subspaces extracted from Fig. 4. Both the experimental results and the theoretical predictions are shown for the state before and after the filter. The theoretical predictions before the filter are based on the state $(|\Psi_1^-\rangle + |\Psi_2^+\rangle + |\Psi_3^-\rangle)/\sqrt{3}$, whereas the predictions after the filter are based on the state $(|\Psi_1^-\rangle + |\Psi_3^-\rangle)/\sqrt{2}$. The ℓ = 1 and ℓ = 3 subspaces remain unchanged through the filter, besides trace normalization factors: before, each represents approximately a third of the state, whereas after, each represents approximately half of the state. The ℓ = 2 subspace, on the other hand, is reduced to near-zero trace: before, it represents approximately a third of the state, whereas after, it represents less than 2% of the state.

To quantify the performance of the filter, we obtain the density matrices of the subspaces ρ_ℓ by tracing over all other OAM values. The trace of ρ_ℓ provides the probability of projecting onto a particular subspace spanned by the states with OAM values $\pm\ell$ (see Table 1 for the numerical values). We see that the probability of projecting onto the ℓ = 2 subspace has changed from 31.9 ± 0.2% before the filter to 1.8 ± 0.1% after the filter. This corresponds to 3.8 ± 0.2% of the original signal and is a clear demonstration of effective filtering of the symmetric contribution to the high-dimensional state. Because of noise, we find that there is a small probability of projecting onto a subspace other than ρ_1, ρ_2, and ρ_3, but this is only on the order of 2 to 3%.

DISCUSSION

Although prior work has considered the HOM effect using spatial modes (*23*, *29*–*31*), here we have departed from this by demonstrating high-dimensional state preparation using the HOM effect, and in particular for the OAM basis. Our work combines knowledge of high-dimensional state analysis and the impact of state symmetry on the HOM effect to produce specific high-dimensional states after the beamsplitter without any post-selection other than conditioning on coincidences. This makes our approach easy to implement. In previous work (*23*), it has been shown that the symmetry of a hybrid (multimode) polarization and spatial mode state (Hermite-Gaussian modes were used) affects the HOM interference and that the antisymmetric state produces coincidences. However, in general, the statistics of measurement outcomes do not allow one to reach conclusions on the post-measurement states. This can be seen by noting that there is a one-to-many correspondence between the positive operators that determine the statistics (so-called effects) of a measurement and the operations that represent the state change due to the measurement (*43*). Therefore, only a state tomography, which was carried out here for the first time, can give conclusive proof of the state after the beamsplitter. The HOM effect has been used with OAM to study qubit states by mapping polarization entanglement to OAM (*29*) and to measure the spiral spectrum of entangled biphoton states (*30*, *31*). Our results show that HOM interference can be used to project certain input states onto antisymmetric states that are entangled in four OAM values (quadit entanglement). Moreover, because of the inherent linearity of the projection, these results imply that product states are transformed into quadit entangled states as well, thereby creating higher-dimensional entanglement. The method can generate, in principle, an unlimited degree of entanglement in a photon pair using product states that involve superposition of many spatial modes as input. We note that the alternative way of creating this kind of entanglement by means of nonlinear optics is very inefficient in comparison. Thus, although important prior work exists on HOM interference with spatial modes, none to date have demonstrated high-dimensional quantum state preparation with the technique.

In conclusion, we have demonstrated HOM interference for high-dimensional entangled photon fields using the OAM of photons. Our results illustrate the discrimination of the antisymmetric state from the symmetric triplet for high-dimensional entangled states, requiring only conditioning on coincidences at the detectors. We analyze the density operator from the output of a HOM filter for OAM modes, which shows effective filtering of the antisymmetric component of a high-dimensional space and the separation of the odd and even OAM states, demonstrating that HOM interference can be used to generate entanglement and engineer the quantum state of OAM entangled photons. This increases the feasibility of applications of the HOM effect to higher-dimensional OAM qudit states. In particular, this filtering step is necessary for higher-dimensional quantum teleportation, a crucial process for long-distance quantum communication with qudits.

MATERIALS AND METHODS

We show the experimental setup in Fig. 1. A 350-mW laser with a wavelength of 355 nm was used to pump a β-barium borate (BBO) crystal to produce degenerate photon pairs (labeled A and B) entangled in their OAM degree of freedom with type I phase matching by SPDC (*44*). The photon in path A is reflected off a right-angle prism mounted on a translational stage that is used to adjust the path length. Path B has two Dove prisms that can be rotated to change the phase of the OAM entangled state to produce $|\Psi_\ell\rangle$. Optionally, we can insert a third Dove prism to produce $|\Phi_\ell\rangle$.

The photons were then passed through the HOM filter, which consists of a 50:50 beamsplitter and two mirrors. After the filter, the photons were incident on SLMs, which, in combination with SMFs, allowed us to make joint projective measurements of particular spatial modes. The SLMs allowed us to consider both two-dimensional subspaces, for example, where the value of ℓ is restricted to ±1, ±2, or ±3, and high-dimensional state spaces, for example, $d_1|\Psi_1^-\rangle + c_2|\Psi_2^+\rangle + d_3|\Psi_3^-\rangle$. The techniques to achieve this can be found in Agnew *et al.* (*42*).

An interference filter with $\Delta\lambda$ = 10 nm was used to select out photons around 710 nm just before the SMFs. The SMFs were connected

to avalanche photodiodes to detect the single photons, and coincidences were registered via a coincidence counter. To maximize the coincidence count rate, we imaged the photon pairs from the plane of the BBO crystal onto the SLMs and then from the SLMs onto the SMFs. We also adjusted the angle of the BBO crystal such that the photon pairs are produced in slightly noncollinear paths (the dip in the ring of light being just visible), because we find that this produces around 1.5 times more coincidence counts compared to when the photons are produced collinearly or noncollinearly. The photon statistics follow a Poisson distribution, and thus, small uncertainties are achieved by accumulating many counts by time-averaging the coincidences. An overview of the entire experiment to achieve coincidences in an SPDC experiment with SLMs is given in McLaren *et al.* (*44*).

SUPPLEMENTARY MATERIALS

Supplementary material for this article is available at http://advances.sciencemag.org/cgi/content/full/2/2/e1501165/DC1
Text

REFERENCES AND NOTES

1. H. Bechmann-Pasquinucci, A. Peres, Quantum cryptography with 3-state systems. *Phys. Rev. Lett.* **85**, 3313–3316 (2000).
2. N. J. Cerf, M. Bourennane, A. Karlsson, N. Gisin, Security of quantum key distribution using *d*-level systems. *Phys. Rev. Lett.* **88**, 127902 (2002).
3. D. Bruß, C. Macchiavello, Optimal eavesdropping in cryptography with three-dimensional quantum states. *Phys. Rev. Lett.* **88**, 127901 (2002).
4. R. T. Thew, A. Acín, H. Zbinden, N. Gisin, Bell-type test of energy-time entangled qutrits. *Phys. Rev. Lett.* **93**, 010503 (2004).
5. M. N. OSullivan-Hale, I. A. Khan, R. W. Boyd, J. C. Howell, Pixel entanglement: Experimental realization of optically entangled $d = 3$ and $d = 6$ qudits. *Phys. Rev. Lett.* **94**, 220501 (2005).
6. A. Mair, A. Vaziri, G. Weihs, A. Zeilinger, Entanglement of the orbital angular momentum states of photons. *Nature* **412**, 313–316 (2001).
7. J. Romero, D. Giovannini, M. G. Mclaren, E. J. Galvez, A. Forbes, M. J. Padgett, Orbital angular momentum correlations with a phase-flipped Gaussian mode pump beam. *J. Opt.* **14**, 085401 (2012).
8. M. McLaren, M. Agnew, J. Leach, F. S. Roux, M. J. Padgett, R. W. Boyd, A. Forbes, Entangled Bessel-Gaussian beams. *Opt. Express* **20**, 23589–23597 (2012).
9. M. Krenn, R. Fickler, M. Huber, R. Lapkiewicz, W. Plick, S. Ramelow, A. Zeilinger, Entangled singularity patterns of photons in Ince-Gauss modes. *Phys. Rev. A* **87**, 012326 (2013).
10. P. G. Kwiat, H. Weinfurter, Embedded Bell-state analysis. *Phys. Rev. A* **58**, R2623–R2626 (1998).
11. J. T. Barreiro, N. K. Langford, N. A. Peters, P. G. Kwiat, Generation of hyperentangled photon pairs. *Phys. Rev. Lett.* **95**, 260501 (2005).
12. G. Molina-Terriza, J. P. Torres, L. Torner, Twisted photons. *Nat. Phys.* **3**, 305–310 (2007).
13. S. Franke-Arnold, L. Allen, M. Padgett, Advances in optical angular momentum. *Laser Photon. Rev.* **2**, 299–313 (2008).
14. M. Mafu, A. Dudley, S. Goyal, D. Giovannini, M. McLaren, M. J. Padgett, T. Konrad, F. Petruccione, N. Lütkenhaus, A. Forbes, Higher-dimensional orbital-angular-momentum-based quantum key distribution with mutually unbiased bases. *Phys. Rev. A* **88**, 032305 (2013).
15. S. K. Goyal, T. Konrad, Teleporting photonic qudits using multimode quantum scissors. *Sci. Rep.* **3**, 3548 (2013).
16. S. Goyal, P. E. Boukama-Dzoussi, S. Ghosh, F. S. Roux, T. Konrad, Qudit-teleportation for photons with linear optics. *Sci. Rep.* **4**, 4543 (2014).
17. X.-L. Wang, X.-D. Cai, Z.-E. Su, M.-C. Chen, D. Wu, L. Li, N.-L. Liu, C.-Y. Lu, J.-W. Pan, Quantum teleportation of multiple degrees of freedom of a single photon. *Nature* **518**, 516–519 (2015).
18. T. M. Graham, H. J. Bernstein, T.-C Wei, M. Junge, P. G. Kwiat, Superdense teleportation using hyperentangled photons. *Nat. Commun.* **6**, 7185 (2015).
19. H.-J. Briegel, W. Dür, J. I. Cirac, P. Zoller, Quantum repeaters: The role of imperfect local operations in quantum communication. *Phys. Rev. Lett.* **81**, 5932–5935 (1998).
20. C. K. Hong, Z. Y. Ou, L. Mandel, Measurement of subpicosecond time intervals between two photons by interference. *Phys. Rev. Lett.* **59**, 2044–2046 (1987).
21. D. Bouwmeester, J.-W. Pan, K. Mattle, M. Eible, H. Weinfurter, A. Zeilinger, Experimental quantum teleportation. *Nature* **390**, 575–579 (1997).
22. A. Fedrizzi, T. Herbst, M. Aspelmeyer, M. Barbieri, T. Jennewein, A. Zeilinger, Anti-symmetrization reveals hidden entanglement. *New J. Phys.* **11**, 103052 (2009).
23. S. P. Walborn, A. N. de Oliveira, S. Pádua, C. H. Monken, Multimode Hong-Ou-Mandel interference. *Phys. Rev. Lett.* **90**, 143601 (2003).
24. P. G. Kwiat, A. M. Steinberg, R. Y. Chiao, Observation of a "quantum eraser": A revival of coherence in a two-photon interference experiment. *Phys. Rev. A* **45**, 7729–7739 (1992).
25. T. B. Pittman, D. V. Strekalov, A. Migdall, M. H. Rubin, A. V. Sergienko, Y. H. Shih, Can two-photon interference be considered the interference of two photons? *Phys. Rev. Lett.* **77**, 1917–1920 (1996).
26. E. Karimi, D. Giovannini, E. Bolduc, N. Bent, F. M. Miatto, M. J. Padgett, R. W. Boyd, Exploring the quantum nature of radial degree of freedom of a photon via Hong-Ou-Mandel interference. *Phys. Rev. A* **89**, 013829 (2014).
27. D. Giovannini, J. Romero, M. J. Padgett, Interference of probability amplitudes: A simple demonstration within the Hong-Ou-Mandel experiment. *J. Opt.* **16**, 032002 (2014).
28. R. Kaltenbaek, B. Blauensteiner, M. Żukowski, M. Aspelmeyer, A. Zeilinger, Experimental interference of independent photons. *Phys. Rev. Lett.* **96**, 240502 (2006).
29. E. Nagali, F. Sciarrino, F. De Martini, L. Marrucci, B. Piccirillo, E. Karimi, E. Santamato, Quantum information transfer from spin to orbital angular momentum of photons. *Phys. Rev. Lett.* **103**, 013601 (2009).
30. W. H. Peeters, E. J. K. Verstegen, M. P. van Exter, Orbital angular momentum analysis of high-dimensional entanglement. *Phys. Rev. A* **76**, 042302 (2007).
31. H. Di Lorenzo Pires, H. C. B. Florijin, M. P. van Exter, Measurement of the spiral spectrum of entangled two-photon states. *Phys. Rev. Lett.* **104**, 020505 (2010).
32. R. J. Lewis-Swan, K. V. Kheruntsyan, Proposal for demonstrating the Hong–Ou–Mandel effect with matter waves. *Nat. Commun.* **5**, 3752 (2014).
33. P. Kok, B. Lovett, *Introduction to Optical Quantum Information Processing* (Cambridge Univ. Press, Cambridge, 2010).
34. P. Kok, W. J. Munro, K. Nemoto, T. C. Ralph, J. P. Dowling, G. J. Milburn, Linear optical quantum computing with photonic qubits. *Rev. Mod. Phys.* **79**, 135–174 (2007).
35. M. Ricci, F. Sciarrino, C. Sias, F. De Martini, Teleportation scheme implementing the universal optimal quantum cloning machine and the universal NOT gate. *Phys. Rev. Lett.* **92**, 047901 (2004).
36. W. T. M. Irvine, A. Lamas Linares, M. J. A. de Dood, D. Bouwmeester, Optimal quantum cloning on a beam splitter. *Phys. Rev. Lett.* **92**, 047902 (2004).
37. E. Nagali, L. Sansoni, F. Sciarrino, F. De Martini, L. Marrucci, B. Piccirillo, E. Karimi, E. Santamato, Optimal quantum cloning of orbital angular momentum photon qubits through Hong–Ou–Mandel coalescence. *Nat. Photon.* **3**, 720–723 (2009).
38. E. Nagali, D. Giovannini, L. Marrucci, S. Slussarenko, E. Santamato, F. Sciarrino, Experimental optimal cloning of four-dimensional quantum states of photons. *Phys. Rev. Lett.* **105**, 073602 (2010).
39. H. P. Specht, J. Bochmann, M. Mücke, B. Weber, E. Figueroa, D. L. Moehring, G. Rempe, Phase shaping of single-photon wave packets. *Nat. Photon.* **3**, 469–472 (2009).
40. M. Agnew, J. Z. Salvail, J. Leach, R. W. Boyd, Generation of orbital angular momentum Bell states and their verification via accessible nonlinear witnesses. *Phys. Rev. Lett.* **111**, 030402 (2013).
41. Z. Y. J. Ou, *Multi-photon Quantum Interference* (Springer, New York, 2007).
42. M. Agnew, J. Leach, M. McLaren, F. S. Roux, R. W. Boyd, Tomography of the quantum state of photons entangled in high dimensions. *Phys. Rev. A* **84**, 062101 (2011).
43. P. Busch, M. Grabowski, J. Lahti, *Operational Quantum Physics* (Springer Verlag, Berlin, Germany, 1995).
44. M. G. McLaren, F. S. Roux, A. Forbes, Realising high-dimensional quantum entanglement with orbital angular momentum. *S. Afr. J. Sci.* **111**, 1–9 (2015).

Acknowledgments

Funding: This work was supported by the Council for Scientific and Industrial Research (CSIR) and the National Research Foundation of South Africa. **Author contributions:** A.F., J.L., F.S.R., and T.K. conceived the research. Y.Z. performed the experiment. Y.Z., F.S.R., and T.K. wrote the theory. Y.Z., M.A., and J.L. conducted the analyses. All authors wrote the manuscript. **Competing interests:** The authors declare that they have no competing interests. **Data and materials availability:** All data needed to evaluate the conclusions in the paper are present in the paper and/or the Supplementary Materials. Additional data related to this paper will be made available by the authors upon request.

Submitted 25 August 2015
Accepted 11 December 2015
Published 26 February 2016
10.1126/sciadv.1501165

Citation: Y. Zhang, F. S. Roux, T. Konrad, M. Agnew, J. Leach, A. Forbes, Engineering two-photon high-dimensional states through quantum interference. *Sci. Adv.* **2**, e1501165 (2016).

Engineering two-photon high-dimensional states through quantum interference

Yingwen Zhang, Filippus S. Roux, Thomas Konrad, Megan Agnew, Jonathan Leach and Andrew Forbes

Sci Adv **2** (2), e1501165.
DOI: 10.1126/sciadv.1501165